

Visualizing delocalized quasiparticles in the vortex state of NbSe₂

Jian-Feng Ge,¹ Koen M. Bastiaans,² Jiasen Niu,¹ Tjerk Benschop,¹ Maialen Ortego Larrazabal,³ Milan P. Allan^{1*}

¹ Leiden Institute of Physics, Leiden University, 2333 CA Leiden, The Netherlands

² Department of Quantum Nanoscience, Kavli Institute of Nanoscience, Delft University of Technology, 2628 CJ Delft, The Netherlands

³ Debye Institute for Nanomaterials Science, Utrecht University, 3508 TA Utrecht, The Netherlands

*Corresponding author. Email: allan@physics.leidenuniv.nl

Bogoliubov quasiparticles play a crucial role in understanding the behavior of a superconductor at the nanoscale, particularly in a vortex lattice where they are thought to be confined to the vortex cores. Here, we use scanning tunneling noise microscopy, which can locally quantify quasiparticles by measuring the effective charge, to observe and image delocalized quasiparticles around vortices in NbSe₂ for the first time. Our data reveals a strong spatial variation of the quasiparticle concentration when tunneling into the vortex state. We find that quasiparticle poisoning dominates when vortices are less than four times the coherence length apart. Our results set a new length scale for quasiparticle poisoning in vortex-based Majorana qubits and yield information on the effect of vortices in quantum circuits. Finally, we can describe our findings within the Ginzburg-Landau framework, but the microscopic origin of the far-extending quasiparticles is yet to be understood.

INTRODUCTION

In a type-II superconductor, the ground state is altered by a finite external magnetic field when its magnitude surpasses the lower critical field value, leading to the formation of an array of vortices that hold quantized magnetic flux. Vortices are topological line defects of the superconducting order parameter $\Psi = \psi e^{i\chi}$. Its phase χ winds (multiple of) 2π around the center of a vortex where the amplitude ψ vanishes^[1]. The supercurrent, generated by the gradient of χ in response to the magnetic field, brings about the emergence of low-energy Bogoliubov quasiparticles localized in the vortices^[2]. Intuitively, quasiparticles are capable of delocalizing from the vortex core due to the fact that the supercurrent decays with a length scale (penetration

depth, λ) that – in most superconductors – exceeds the radius of the vortex core (which scales with the coherence length, ξ).

Indeed, signatures of delocalized quasiparticles have been observed even in conventional s -wave superconductors. For example, early magnetotransport experiments implied the existence of residual quasiparticles in NbSe_2 ^[3] and $\text{YNi}_2\text{B}_2\text{C}$ ^[4] having a cyclotron radius much larger than ξ . Later heat transport measurements^[5–7] probed these delocalized quasiparticles, because they can move from one vortex to another and thus enable macroscopic heat transport in the thermally insulating superconductor^[8,9]. However, a direct, local observation of delocalized quasiparticles in vortex matter is still absent. In this work, we will locally investigate these delocalized quasiparticles by measuring shot noise in a scanning tunneling microscope.

Shot noise is proportional to the charge of the carriers q and the average current $|I|$, $S = 2q|I|$. Therefore, shot noise offers a direct and sensitive method, via the charge q , to investigate delocalized quasiparticles within a bath of electronic pairs. In the absence of quasiparticles, when the applied bias falls within the superconducting gap energy, the tunneling current into a superconductor is solely coming from Andreev reflections. The Andreev reflection process, i.e., a tunneling electron is reflected as a hole, transfers effectively two electron charge ($q = 2e$), leading to the Andreev current I_{2e} . In contrast, direct tunneling into a quasiparticle state with current I_{1e} simply transfers one electron charge ($q = 1e$). In the framework of the tunneling Hamiltonian approach^[10], when the transparency of the tunnel junction is small, $\tau \ll 1$, the two current contributions are formulated as

$$I_{ne} \propto n \tau^n / 4^{n-1}, \quad n = 1, 2. \quad (1)$$

When a finite amount of quasiparticles exist within the gap, the total current is composed of the quasiparticle current and the Andreev current (neglecting higher-order Andreev), $I = I_{1e} + I_{2e}$. The shot noise can then be expressed as $S = 2q^*|I|$, with q^* as the overall effective charge that can take any value between $1e$ and $2e$. Because of their different weights in transparency τ , q^* is extremely sensitive to a small portion of quasiparticles, which may not be detectable in the total current I . For example, as simulated in Fig. 1b, for $\tau = 5 \times 10^{-4}$, 1% of quasiparticles lower the effective charge significantly, from $2e$ to $1.20e$.

RESULTS

Here, we employ this extreme sensitivity to quasiparticles by using scanning tunneling shot noise spectroscopy (Fig. 1a) to visualize delocalized quasiparticles in NbSe₂. We cleave single crystals of 2H-NbSe₂ in an ultrahigh vacuum and immediately load it in our scanning tunneling microscope (STM) at a temperature $T = 2.3$ K. We first measure spatially resolved differential conductance, a standard method to image the vortex lattice in NbSe₂. Throughout this work, we use a superconducting tip with an energy gap $\Delta_t = 1.3$ meV to achieve an enhanced energy resolution, and the local density of states (DOS) of the NbSe₂ sample can be obtained by a standard deconvolution procedure^[11,12].

As shown in Fig. 2a, the differential conductance map at $eV_{\text{bias}} = \Delta_t$, which corresponds to the sample DOS at the Fermi level, shows a triangular lattice of vortices in an external magnetic field $B = 0.1$ T. In the vortex core a substantial enhancement of the DOS is understood as bound states formed by localized quasiparticles, first brought up by Caroli, de Gennes, and Matricon^[13], while outside the vortex in the midpoint between two neighboring vortices, the differential conductance spectrum hardly differs from that measured at $B = 0$ T (Fig. 2d). At the bias energy $eV_{\text{bias}} = \Delta_t$, the difference in differential conductance between $B = 0$ T and outside the vortex at $B = 0.1$ T is smaller than the error bar of our measurements, which hinders us from detecting residual quasiparticles directly from tunneling conductance.

We now use the noise measurements introduced above, to determine the quasiparticle contributions to the tunneling current. The current noise measured at $B = 0$ T (Fig. 2e) follows the $q^* = 1e$ line when $|eV_{\text{bias}}| > \Delta_t + \Delta_s$ – as expected, because quasiparticles are available outside the gap. When the bias is lowered below the gap energy, $|eV_{\text{bias}}| < \Delta_t + \Delta_s$, the noise develops a broadened step transition towards the $q^* = 2e$ curve, indicating that only the Andreev processes contribute to the current and virtually no quasiparticles remain. On the other hand, in a finite field $B = 0.1$ T at the midpoint between two neighboring vortices, the measured shot noise shows a transition departing the $q^* = 1e$ curve for $|eV_{\text{bias}}| < \Delta_t + \Delta_s$, but not reaching the $q^* = 2e$ curve, meaning that a finite fraction of quasiparticle tunneling persists in parallel with the Andreev current. We numerically extract the effective charge q^* for the two cases in Fig. 2f, and find that the transition within the gap is sharper and reaches a plateau of $2e$ for $B = 0$ T, while for $B = 0.1$ T, it is broader and only plateaus at $1.65e$ outside the vortex at $eV_{\text{bias}} = \Delta_t$, yielding a portion of 0.14% zero-energy quasiparticles delocalized from the vortex cores. Note that the differential conductance measurements (Fig. 2d) for the two cases look nearly the same, emphasizing the additional information obtained with shot noise spectroscopy.

Next, we image both localized and delocalized quasiparticles in a vortex lattice by spatially resolved shot-noise imaging. Inside the vortex cores, we expect the localized quasiparticles to allow single-electron tunneling, leading to $q^* = 1e$ [12]. Away from the vortex cores, we expect the density of quasiparticles to drastically decrease and q^* to increase above $1e$ because Andreev reflections contribute to the tunneling current. Therefore, a clear contrast in shot noise is expected between tunneling in and outside the vortex cores. This is exactly what we observe in Fig. 2b, where we measure shot noise for a constant current, in active feedback, at a fixed bias energy in an area containing 8 vortices. We chose the same field of view as the vortex lattice in Fig. 2a, which is imaged at the same bias. The resulting spatially resolved effective charge q^* map (Fig. 2c) reveals the concentration of quasiparticles, where a darker color indicates an effective charge closer to $1e$, and thus more quasiparticles, while a lighter color indicates an effective charge closer to $2e$, and thus less quasiparticles. We observe more quasiparticles in the vortex cores, as expected.

Individual vortices in NbSe_2 have a peculiar six-fold star shape (Fig. 3), which we can compare with spatial shot noise maps^[14]. First, as a consistency test, we extract the spatial dependence of the dynamic junction impedance R_{dyn} from our measurements, which is related to the differential conductance measured in active feedback, and thus shows a six-fold star shape in the maps and radial-average plots consistent with the density of state data (Figs. 3b,d,e). However, our shot noise data around the same vortex in Fig. 3c shows an almost isotropic structure. Within our resolution, the radial-average plot of noise (Fig. 3f) yields a six-fold anisotropic [$\sin(6\theta)$] term two orders of magnitude smaller than that of differential conductance (Fig. 3d). We can explain this discrepancy from the higher sensitivity of the shot noise map to quasiparticle tunneling than Andreev process. Fig. 1b illustrates that the effective charge already reaches below $1.05e$ when the quasiparticles are contributing more than 5%. Therefore, when quasiparticle tunneling contribution varies from 5% to 100%, the effective charge only changes by 5%.

Finally, we turn to the spatial dependence of quasiparticle concentration between vortices, which is the main focus of this study. We take high-resolution shot noise map around 3 vortices at $B = 40$ mT, as shown in Fig. 4. We extract the effective charge $q^*(r)$ at $eV_{\text{bias}} = \Delta_t$, where r is the distance along line cuts between two vortex cores in Fig. 4a. We observe that $q^*(r)$ increases from $1e$ at core centers on both sides ($r = 0$ and $r = d$) to a maximum of $1.78e$, where d is the inter-vortex distance. The maximal q^*_{max} appears at the midpoint between vortices at r

$= d/2 = 94$ nm, where the concentration of delocalized quasiparticles is lowest, or the concentration of pairs is the highest. We can describe this spatial dependence with a Ginzburg-Landau model in the limit of individual, isolated vortices, if we make a simple assumption that the effective charge q^* is proportional to the pair density. With only one fitting parameter, the coherence length, $\xi = 12$ nm^[15], we can obtain a good quantitative agreement between our effective charge profile and our Ginzburg-Landau model (see Methods for details of our model).

DISCUSSION

The absence of residual quasiparticles at $B = 0$ T indicates that the external magnetic field is the cause of both the localized (in the vortex core) and delocalizing quasiparticles (between the vortex cores). The question therefore arises how the spatial distribution of delocalized quasiparticles depends on magnetic field strength B . We carry out shot noise spectroscopy and extract the maximal $q_{\max}^* = q^*(r=d/2)$ at the midpoint between vortices at several different field strengths in Fig. 4c. We observe that q_{\max}^* decreases with increasing B starting even before our lowest measured field 40 mT. This observation directly confirms the implication that delocalized quasiparticles present throughout the vortex state of NbSe₂, leading to an onset of increasing thermal conductivity right above the lower critical field $B_{c1} = 20$ mT^[7]. Further, our Ginzburg-Landau model fits the magnetic field dependence of q_{\max}^* excellently, and it shows that at $B^* \sim 1.0$ T, q_{\max}^* reaches $1e$ where quasiparticle current dominates the tunneling process in the entire sample.

A ramification of our study is that there is a field B^* , much smaller than the upper critical field $B_{c2} = 4.0$ T at $T = 2.3$ K^[16], which indicates the emergence of a vortex state with highly delocalized quasiparticles between vortices. Our model also defines a different length scale $\xi^* \sim 4\xi$: for intervortex distance $d < \xi^* = 4\xi$, quasiparticles delocalize from one vortex and reach a neighboring vortex, and thus spread throughout the space between vortices. We emphasize that this length scale ξ^* determines a limit for inter-vortex distance, below which quasiparticle current dominates. However, even when vortices are farther apart than ξ^* , delocalized quasiparticles still exist between vortices. For instance, at $d = 1.4 \xi^*$ ($B = 0.5 B^*$), q_{\max}^* already decreases to $1.2e$, corresponding to a quasiparticle contribution of one percent.

Our findings are relevant to understanding quasiparticle poisoning in vortex-based Majorana bound states. Majorana bound states are predicted to exist in vortex cores of topological superconductors, appearing as a zero-bias peak in tunneling differential

conductance^[17]. Zero-bias peaks have only been reported in a fraction of vortices of Fe-based superconductor $\text{FeTe}_{0.55}\text{Se}_{0.45}$ ^[18,19]. In these reports, the intervortex distance is usually less than 30 nm, comparable to $\zeta^* = 4\zeta = 12\text{--}15$ nm for $\text{FeTe}_{0.55}\text{Se}_{0.45}$. There is still controversy about whether the zero-bias peaks originate from Majorana bound states^[12,20,21], and local shot noise spectroscopy at low temperatures may be able to confirm this^[12]. Nevertheless, even if there were Majorana bound states in the vortex cores, our results show that zero-energy quasiparticles on the order of 1% can still hop between vortices. This is crucial for the application of the topological qubits made of these Majorana-carrying vortices, because the readout of topological qubits relies on the total charge of vortices^[22\text{--}24], and the uncontrollable transfer of zero-energy quasiparticles between vortices can frequently alter the state of a qubit. Therefore, our results set a hard limit for using vortex-based Majorana bound states, characterized by $\zeta^* \sim 4\zeta$; below this length scale, quasiparticle poisoning prevails.

Even though we can have a good agreement between our data and our Ginzburg-Landau model, we still lack a microscopic understanding of where these delocalized quasiparticles between vortices come from. Two possible theories exist to describe the delocalization of quasiparticles from vortex cores. First, vortices form a lattice to minimize their total free energy, i.e., the interaction among them, which is mediated by quasiparticles tunneling from one to another^[8]. However, this tunneling probability, or the (residual) density of Bogoliubov quasiparticles, which scales with magnetic field strength, does not agree with our observation as shown by comparing our data to the intervortex tunneling (IVT) model in Fig. 4c (brown curve, based on Eq. 4 of Ref. [9]). Second, when Cooper pairs acquire a large enough momentum, e.g., by applying a sufficiently large (super)current, they break into in-gap or even zero-energy Bogoliubov quasiparticles, known as the Volovik effect^[25] or Doppler-shift effect^[26\text{--}29]. These Bogoliubov quasiparticles, having momenta mainly along the current direction, can even form a Fermi surface^[29]. In our case, as we measure at $eV_{\text{bias}} = \Delta_t$ (i.e. at the Fermi level of the NbSe_2), the Doppler-shift energy to close the gap would be on the order of Δ_s , corresponding to a supercurrent close to the critical current that only appears near the core center^[28]. However, our result is still in line with the Volovik effect, in the sense that even much lower than the critical current, the circulating supercurrent still does break a small amount of Cooper pairs into delocalized quasiparticles^[30]. Because the critical current decays on the length scale of penetration depth, which is greater than coherence length in type-II superconductors such as NbSe_2 , the zero-energy delocalized quasiparticles can reach far from vortex cores (Fig. 4).

In summary, we measured the first spatially resolved image of delocalized quasiparticles in superconductor NbSe_2 by scanning tunneling shot noise microscopy. Our results show that delocalized quasiparticles spread across the vortex lattice when the inter-vortex distance is less than four times the coherence length, which sets a new length scale for quasiparticle poisoning in vortex-based Majorana qubits. More generally, our technique provides a new platform for investigating trivial and exotic quasiparticles in conventional and unconventional superconductors. For example, the ability to visualize these delocalized quasiparticles can aid in determining the pairing symmetry of the superconductor, because quasiparticles tend to be more delocalized from vortices in superconductors with gapless nodes on the Fermi surface^[25,31–34]. Furthermore, our technique also allows real-space detection of quasiparticle delocalization across the predicted phase boundary between a superconductor with a metallic nonsuperconducting ground state and one with an insulating ground state^[35].

MATERIALS AND METHODS

Sample preparation and STM measurements

The 2H- NbSe_2 samples ($T_c = 7.2$ K) are purchased from HQ Graphene. The samples with a thickness of ~ 0.5 mm are cleaved in an ultrahigh vacuum at ~ 30 K and immediately inserted into a customized STM (USM-1500, Unisoku Co., Ltd). All measurements are performed in a cryogenic vacuum at a base temperature of $T = 2.3$ K. Prior to all the measurements, a Pt-Ir tip is made superconducting by indenting it into a clean $\text{Pb}(111)$ surface. We perform scanning tunneling spectroscopy using standard lock-in techniques without the feedback loop enabled. A bias voltage modulation at a frequency of 887 Hz with an amplitude of 100 μV (for maps around vortex) or 50 μV (for high-resolution point spectra) is applied. Our superconducting tip exhibits a critical field of about 0.7 T, deducted from differential conductance measurements in different magnetic fields on an atomically flat $\text{Au}(111)$ surface^[12].

Noise measurements

We perform noise spectroscopy at a constant junction resistance R_J in a slow feedback loop when varying the bias voltage V_{bias} (and hence tunneling current $I = V_{\text{bias}}/R_J$) using our custom-built cryogenic megahertz amplifier developed recently. The amplifier consists of an LC tank circuit and a high-electron-mobility transistor that converts the current fluctuations in the junction into voltage fluctuations across a 50 Ohm line, as described in detail in Ref. [36]. To

extract the effective charge transferred in the junction we follow the same procedure as in Refs. [12,37], described below.

The measured total voltage noise is

$$S_V^{\text{meas}}(\omega, V) = G^2 |Z_{\text{tot}}|^2 S_I, \quad (2)$$

where G is the total gain calibrated by a current noise spectrum at a high bias, Z_{tot} is the impedance of our system, and S_I is the total current noise

$$S_I = 2q^* I \coth\left(\frac{q^* V}{2k_B T}\right) + \frac{4k_B T R_{\text{res}}}{|Z_{\text{tot}}|^2} + S_{\text{amp}} \quad (3)$$

The first term is the junction noise including thermal noise and shot noise, the second term is the thermal noise originating from the resistive part R_{res} of the LC resonator circuit, and S_{amp} is the intrinsic current noise of our amplifier.

As the first step of the procedure, we measure the background noise by retracting the tip out of tunneling ($I=0$ so the first term vanishes), which gives $4k_B T R_{\text{res}}/|Z_{\text{res}}|^2 + S_{\text{amp}}$, where $Z_{\text{tot}} = Z_{\text{res}}$ because the junction is an open circuit. Then we measure noise in tunneling and subtract the background noise (for typical values of R_J in the MOhm regime we also consider Z_{tot} in the second term, as Z_{res} is in parallel with R_J). Thus, we can obtain the current noise coming from the junction. Finally, we numerically extract the q^* value at each bias.

Ginzburg-Landau (GL) model

In principle the standard GL equation is only valid near T_c ; for arbitrary $T < T_c$ one can solve the quasiclassical Eilenberger equations to obtain the exact solution, or one can incorporate the temperature effect in the extended GL equations^[38]. For simplicity, we use the solution of the GL equations for a lattice of isolated vortices, where the order parameter ψ around each isolated vortex has a spatial decay over a distance r from the center of the vortex core, in the approximate form of^[28]

$$\psi(r) = \psi(r = \infty) \tanh\left(\sqrt{\frac{3}{8}} \frac{r}{\xi}\right). \quad (4)$$

The density of condensed pairs is $ns(r) = |\psi(r)|^2$, and then we assume effective charge is proportional to the pair density over the vortex lattice, which is the sum of ns from individual vortices

$$q^*(r) \propto \sum_{i=1}^n n_s(r - r_{ci}) \quad (5)$$

where r_{Ci} locates the core center of the i -th vortex. The maximum of $q^*(r)$ at a certain field B , $q^*(r=d/2)$, is determined by magnetic flux quantum enclosed in the area of a single vortex $\Phi_0 = \sin(\pi/3) \cdot Bd^2/2 = 2.068 \times 10^{-15}$ Wb.

REFERENCES

- [1] A. A. Abrikosov, “Nobel Lecture: Type-II superconductors and the vortex lattice,” *Rev. Mod. Phys.* **76**, 975–979 (2004). <http://dx.doi.org/10.1103/RevModPhys.76.975> .
- [2] C. Berthod, “Vorticity and vortex-core states in type-II superconductors,” *Phys. Rev. B* **71**, 134513 (2005). <http://dx.doi.org/10.1103/PhysRevB.71.134513> .
- [3] J. E. Graebner and M. Robbins, “Fermi-Surface Measurements in Normal and Superconducting 2 H -Nb Se 2,” *Phys. Rev. Lett.* **36**, 422–425 (1976). <http://dx.doi.org/10.1103/PhysRevLett.36.422> .
- [4] T. Terashima, C. Haworth, H. Takeya, S. Uji, H. Aoki, and K. Kadowaki, “Small superconducting gap on part of the Fermi surface of YNi₂B₂C from the de Haas–van Alphen effect,” *Phys. Rev. B* **56**, 5120–5123 (1997). <http://dx.doi.org/10.1103/PhysRevB.56.5120> .
- [5] K. Izawa, A. Shibata, Y. Matsuda, Y. Kato, H. Takeya, K. Hirata, C. J. van der Beek, and M. Konczykowski, “Low Energy Quasiparticle Excitation in the Vortex State of Borocarbide Superconductor YNi₂B₂C,” *Phys. Rev. Lett.* **86**, 1327–1330 (2001). <http://dx.doi.org/10.1103/PhysRevLett.86.1327> .
- [6] A. V. Sologubenko, J. Jun, S. M. Kazakov, J. Karpinski, and H. R. Ott, “Thermal conductivity of single-crystalline MgB₂,” *Phys. Rev. B* **66**, 014504 (2002). <http://dx.doi.org/10.1103/PhysRevB.66.014504> .
- [7] E. Boaknin, M. A. Tanatar, J. Paglione, D. Hawthorn, F. Ronning, R. W. Hill, M. Sutherland, L. Taillefer, J. Sonier, S. M. Hayden, and J. W. Brill, “Heat Conduction in the Vortex State of N b S e 2 : Evidence for Multiband Superconductivity,” *Phys. Rev. Lett.* **90**, 117003 (2003). <http://dx.doi.org/10.1103/PhysRevLett.90.117003> .
- [8] M. Ichioka, A. Hasegawa, and K. Machida, “Vortex lattice effects on low-energy excitations in d -wave and s -wave superconductors,” *Phys. Rev. B* **59**, 184–187 (1999). <http://dx.doi.org/10.1103/PhysRevB.59.184> .
- [9] A. A. Golubov and A. E. Koshelev, “Thermal conductivity in the mixed state of a superconductor at low magnetic fields,” *Phys. Rev. B* **83**, 094521 (2011). <http://dx.doi.org/10.1103/PhysRevB.83.094521> .
- [10] J. C. Cuevas, A. Martín-Rodero, and A. L. Yeyati, “Shot Noise and Coherent Multiple Charge Transfer in Superconducting Quantum Point Contacts,” *Phys. Rev. Lett.* **82**, 4086–4089 (1999). <http://dx.doi.org/10.1103/PhysRevLett.82.4086> .
- [11] D. Chatzopoulos, D. Cho, K. M. Bastiaans, G. O. Steffensen, D. Bouwmeester, A. Akbari, G. Gu, J. Paaske, B. M. Andersen, and M. P. Allan, “Spatially dispersing Yu-Shiba-Rusinov states in the unconventional superconductor FeTe_{0.55}Se_{0.45},” *Nat Commun* **12**, 298 (2021). <http://dx.doi.org/10.1038/s41467-020-20529-x> .
- [12] J.-F. Ge, K. M. Bastiaans, D. Chatzopoulos, D. Cho, W. O. Tromp, T. Benschop, J. Niu, G. Gu, and M. P. Allan, “Single-electron charge transfer into putative Majorana and trivial modes in individual vortices,” *Nat Commun* **14**, 3341 (2023). <http://dx.doi.org/10.1038/s41467-023-39109-w> .
- [13] C. Caroli, P. G. De Gennes, and J. Matricon, “Bound Fermion states on a vortex line in a type II superconductor,” *Physics Letters* **9**, 307–309 (1964). [http://dx.doi.org/10.1016/0031-9163\(64\)90375-0](http://dx.doi.org/10.1016/0031-9163(64)90375-0) .

[14] H. F. Hess, R. B. Robinson, and J. V. Waszczak, “Vortex-core structure observed with a scanning tunneling microscope,” *Phys. Rev. Lett.* **64**, 2711–2714 (1990).
<http://dx.doi.org/10.1103/PhysRevLett.64.2711> .

[15] D. E. Prober, R. E. Schwall, and M. R. Beasley, “Upper critical fields and reduced dimensionality of the superconducting layered compounds,” *Phys. Rev. B* **21**, 2717–2733 (1980). <http://dx.doi.org/10.1103/PhysRevB.21.2717> .

[16] A. Nader and P. Monceau, “Critical field of 2H-NbSe₂ down to 50mK,” *SpringerPlus* **3**, 16 (2014). <http://dx.doi.org/10.1186/2193-1801-3-16> .

[17] L. Fu and C. L. Kane, “Superconducting Proximity Effect and Majorana Fermions at the Surface of a Topological Insulator,” *Phys. Rev. Lett.* **100**, 096407 (2008).
<http://dx.doi.org/10.1103/PhysRevLett.100.096407> .

[18] D. Wang, L. Kong, P. Fan, H. Chen, S. Zhu, W. Liu, L. Cao, Y. Sun, S. Du, J. Schneeloch, R. Zhong, G. Gu, L. Fu, H. Ding, and H.-J. Gao, “Evidence for Majorana bound states in an iron-based superconductor,” *Science* **362**, 333–335 (2018).
<http://dx.doi.org/10.1126/science.aoa1797> .

[19] T. Machida, Y. Sun, S. Pyon, S. Takeda, Y. Kohsaka, T. Hanaguri, T. Sasagawa, and T. Tamegai, “Zero-energy vortex bound state in the superconducting topological surface state of Fe(Se,Te),” *Nat. Mater.* **18**, 811–815 (2019). <http://dx.doi.org/10.1038/s41563-019-0397-1> .

[20] S. Zhu, L. Kong, L. Cao, H. Chen, M. Papaj, S. Du, Y. Xing, W. Liu, D. Wang, C. Shen, F. Yang, J. Schneeloch, R. Zhong, G. Gu, L. Fu, Y.-Y. Zhang, H. Ding, and H.-J. Gao, “Nearly quantized conductance plateau of vortex zero mode in an iron-based superconductor,” *Science* **367**, 189–192 (2020).
<http://dx.doi.org/10.1126/science.aax0274> .

[21] B. Jäck, Y. Xie, and A. Yazdani, “Detecting and distinguishing Majorana zero modes with the scanning tunnelling microscope,” *Nat Rev Phys* **3**, 541–554 (2021).
<http://dx.doi.org/10.1038/s42254-021-00328-z> .

[22] A. R. Akhmerov, J. Nilsson, and C. W. J. Beenakker, “Electrically Detected Interferometry of Majorana Fermions in a Topological Insulator,” *Phys. Rev. Lett.* **102**, 216404 (2009). <http://dx.doi.org/10.1103/PhysRevLett.102.216404> .

[23] B. H. November, J. D. Sau, J. R. Williams, and J. E. Hoffman, “Scheme for Majorana Manipulation Using Magnetic Force Microscopy,” *arXiv:1905.09792 [cond-mat]* (2019). [URL: <http://arxiv.org/abs/1905.09792>].

[24] J. F. Steiner and F. Von Oppen, “Readout of Majorana qubits,” *Phys. Rev. Research* **2**, 033255 (2020). <http://dx.doi.org/10.1103/PhysRevResearch.2.033255> .

[25] G. E. Volovik, “Superconductivity with lines of GAP nodes: density of states in the vortex,” *Soviet Journal of Experimental and Theoretical Physics Letters* **58**, 469 (1993).

[26] M. Franz and Z. Tešanović, “Quasiparticle spectra in the vicinity of a *d*-wave vortex,” *Phys. Rev. B* **60**, 3581–3588 (1999). <http://dx.doi.org/10.1103/PhysRevB.60.3581> .

[27] E. Schachinger and J. P. Carbotte, “Doppler shift on local density of states and local impurity scattering in the vortex state,” *Phys. Rev. B* **62**, 592–599 (2000).
<http://dx.doi.org/10.1103/PhysRevB.62.592> .

[28] X. Liu, Y. X. Chong, R. Sharma, and J. C. S. Davis, “Atomic-scale visualization of electronic fluid flow,” *Nat. Mater.* **20**, 1480–1484 (2021).
<http://dx.doi.org/10.1038/s41563-021-01077-1> .

[29] Z. Zhu, M. Papaj, X.-A. Nie, H.-K. Xu, Y.-S. Gu, X. Yang, D. Guan, S. Wang, Y. Li, C. Liu, J. Luo, Z.-A. Xu, H. Zheng, L. Fu, and J.-F. Jia, “Discovery of segmented Fermi surface induced by Cooper pair momentum,” *Science* **374**, 1381–1385 (2021).
<http://dx.doi.org/10.1126/science.abf1077> .

[30] P. Fulde, in *Tunneling Phenomena in Solids*, edited by E. Burstein and S. Lundqvist (Springer US, Boston, MA, 1969), pp. 427–442. http://dx.doi.org/10.1007/978-1-4684-1752-4_29.

[31] S. Kambe, A. D. Huxley, P. Rodière, and J. Flouquet, “Low Field Scaling of the Flux-Flow Resistivity in the Unconventional Superconductor UPt 3,” *Phys. Rev. Lett.* **83**, 1842–1845 (1999). <http://dx.doi.org/10.1103/PhysRevLett.83.1842>.

[32] M. Nohara, M. Isshiki, F. Sakai, and H. Takagi, “Quasiparticle Density of States of Clean and Dirty s -Wave Superconductors in the Vortex State,” *J. Phys. Soc. Jpn.* **68**, 1078–1081 (1999). <http://dx.doi.org/10.1143/JPSJ.68.1078>.

[33] K. A. Moler, D. L. Sisson, J. S. Urbach, M. R. Beasley, A. Kapitulnik, D. J. Baar, R. Liang, and W. N. Hardy, “Specific heat of YBa₂Cu₃O_{7- δ} ,” *Phys. Rev. B* **55**, 3954–3965 (1997). <http://dx.doi.org/10.1103/PhysRevB.55.3954>.

[34] D. G. Hawthorn, S. Y. Li, M. Sutherland, E. Boaknin, R. W. Hill, C. Proust, F. Ronning, M. A. Tanatar, J. Paglione, L. Taillefer, D. Peets, R. Liang, D. A. Bonn, W. N. Hardy, and N. N. Kolesnikov, “Doping dependence of the superconducting gap in Tl₂Ba₂CuO_{6+ δ} from heat transport,” *Phys. Rev. B* **75**, 104518 (2007). <http://dx.doi.org/10.1103/PhysRevB.75.104518>.

[35] S. Vishveshwara, T. Senthil, and M. P. A. Fisher, “Superconducting ‘metals’ and ‘insulators,’” *Phys. Rev. B* **61**, 6966–6981 (2000). <http://dx.doi.org/10.1103/PhysRevB.61.6966>.

[36] K. M. Bastiaans, T. Benschop, D. Chatzopoulos, D. Cho, Q. Dong, Y. Jin, and M. P. Allan, “Amplifier for scanning tunneling microscopy at MHz frequencies,” *Review of Scientific Instruments* **89**, 093709 (2018). <http://dx.doi.org/10.1063/1.5043267>.

[37] K. M. Bastiaans, D. Chatzopoulos, J.-F. Ge, D. Cho, W. O. Tromp, J. M. van Ruitenbeek, M. H. Fischer, P. J. de Visser, D. J. Thoen, E. F. C. Driessens, T. M. Klapwijk, and M. P. Allan, “Direct evidence for Cooper pairing without a spectral gap in a disordered superconductor above T_c ,” *Science* **374**, 608–611 (2021). <http://dx.doi.org/10.1126/science.abe3987>.

[38] A. V. Vagov, A. A. Shanenko, M. V. Milošević, V. M. Axt, and F. M. Peeters, “Extended Ginzburg-Landau formalism: Systematic expansion in small deviation from the critical temperature,” *Phys. Rev. B* **85**, 014502 (2012). <http://dx.doi.org/10.1103/PhysRevB.85.014502>.

[39] M. Ternes, W. D. Schneider, J. C. Cuevas, C. P. Lutz, C. F. Hirjibehedin, and A. J. Heinrich, “Subgap structure in asymmetric superconducting tunnel junctions,” *Phys. Rev. B* **74**, 132501 (2006). <http://dx.doi.org/10.1103/PhysRevB.74.132501>.

ACKNOWLEDGMENTS

We acknowledge C. W. J. Beenakker, C. Bolech, F. van Oppen, V. Geshkenbein, F. Gaggioli, X. Liu, C. Renner, and C. Berthod for valuable discussions.

Funding: This work was supported by the European Research Council (ERC CoG PairNoise). K.M.B. was supported by the Netherlands Organization for Scientific Research (NWO Veni grant VI.Veni.212.019).

Author contributions: J-F.G. and K.M.B. performed the experiments and analyzed the data. All authors contributed to the interpretation of the data and writing of the manuscript. M.P.A. supervised the project.

Competing interests: The authors declare that they have no competing interests.

Data and materials availability: All data in the main text and the supplementary information will be available on Zenodo after publication.

Figures

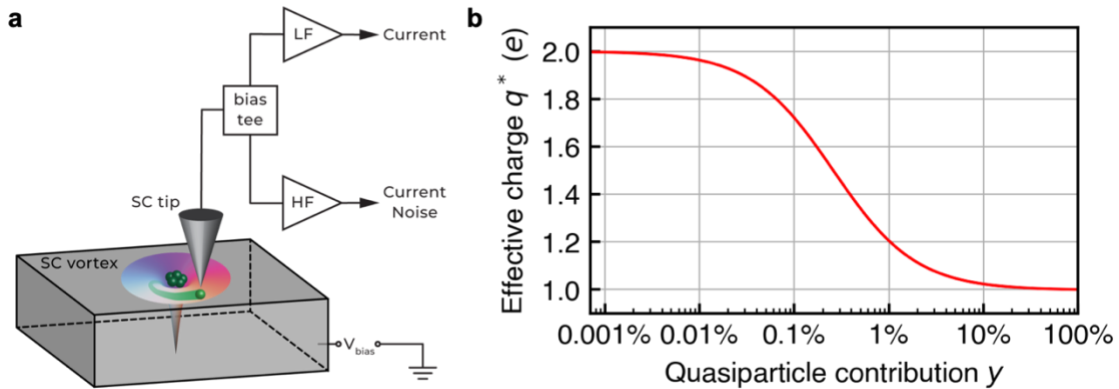


Fig. 1 Visualizing delocalized quasiparticles by scanning tunneling shot noise spectroscopy. **a** Schematic illustration of the scanning tunneling noise microscope setup. A bias voltage V_{bias} is applied between the superconducting (SC) tip and sample. A SC vortex is shown in the sample: the order parameter has a winding phase (color wheel) and a decreasing amplitude (height) inside the vortex core. Green balls illustrate localized quasiparticles (dark color) in the core and delocalized quasiparticles (light color with a trail) outside the core. HF and LF stand for high- and low-frequency amplifiers, respectively. **b** Simulation of effective charge as a function of quasiparticle contribution at a fixed junction transparency $\tau = 5 \times 10^{-4}$. Here the quasiparticle contribution y is defined by the constant of proportionality in Eq. 1 for I_{1e} ($n=1$), i.e., $y = I_{1e}/\tau$, which vanishes in the absence of quasiparticles. The effective charge q^* is extracted numerically by Eq. 3, assuming only the theoretical junction noise (the first term) presents. A constant temperature is set to $T = 2.3$ K.

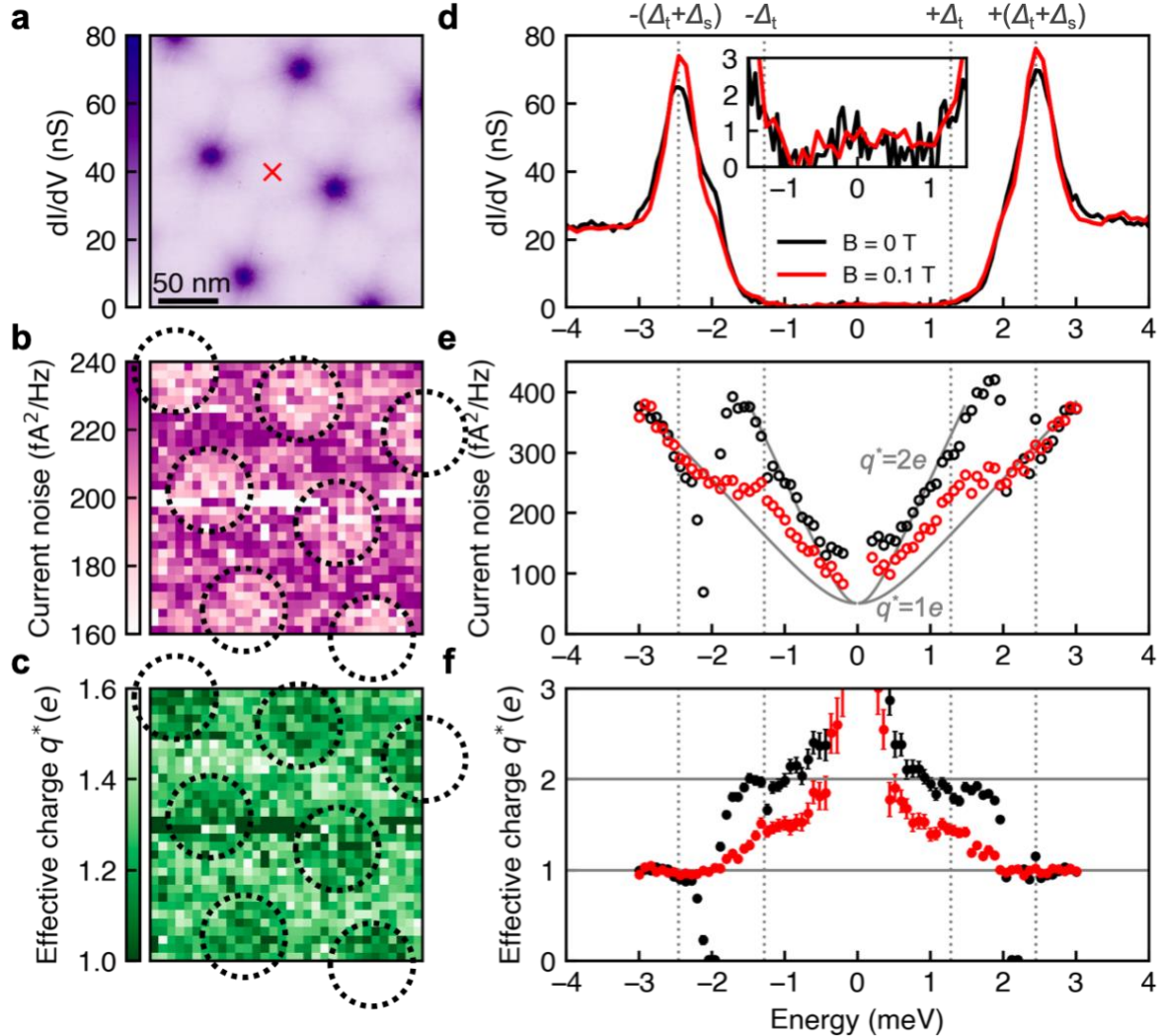


Fig. 2 Differential conductance and noise spectroscopic imaging on vortices of NbSe₂. **a** Differential conductance image measured at $eV_{\text{bias}} = \Delta_t$ and $B = 0.1$ T showing a lattice of vortices. **b** spatially resolved current noise measured at $eV_{\text{bias}} = \Delta_t$ in the same field of view as **a**. **c** effective charge image extracted from **b** by numerically solving Eq. 3. Dotted circles in **b** and **c** indicate the locations of vortices. **d** Differential conductance spectra taken in zero field (black) and $B = 0.1$ T (red, location marked in **a**). The inset shows a zoom-in view of the spectra inside the gap. **e** noise spectra and **f** the extracted effective charge at the same locations as **d**. The gray curves in **e** are the expected junction noise (first term of Eq. 3) with an effective charge q^* of $1e$ and $2e$ at $T = 2.3$ K. The error bars are determined by the fluctuation of the current noise in time, yielding a standard deviation of 9.25 fA²/Hz. The dotted lines in **d-f** indicate peak energies $\pm(\Delta_s + \Delta_t)$ and gap energy of the tip $\pm\Delta_t$. Setup conditions: **a** and **d**, $V_{\text{set}} = 5$ mV, $I_{\text{set}} = 200$ pA; **b**, $V_{\text{set}} = 1.3$ mV, $I_{\text{set}} = 520$ pA, $R_J = 2.5$ MΩ; **e**, $R_J = 2.5$ MΩ.

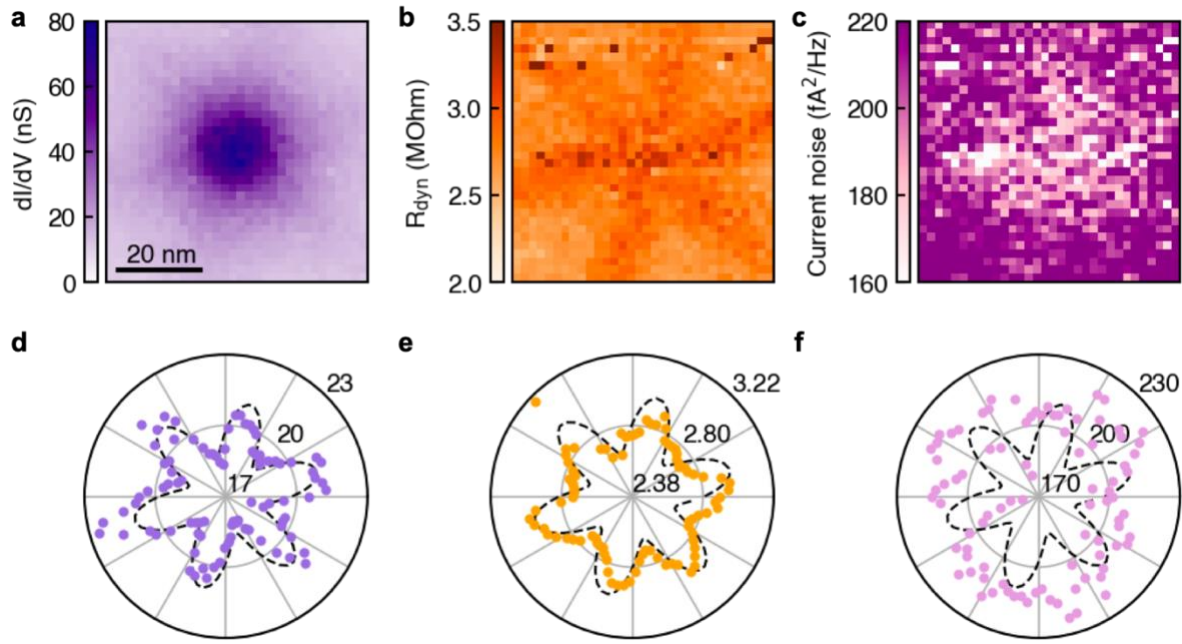


Fig. 3 Core structure of an individual vortex imaged by both differential conductance and noise spectroscopy. **a** Differential conductance image measured at $eV_{bias} = -\Delta_t$ and $B = 0.1$ T showing an individual vortex. **b, c** Dynamic resistance (**b**) and current noise (**c**) imaged at $eV_{bias} = -\Delta_t$ in the same field of view as **a**. **d-f** Radial average of **a-c**, respectively, in the radial range of 19.3 nm – 28.0 nm from the vortex core. The dashed, six-fold star curve $A[1+0.06 \sin(6\theta)]$ serves as a guide to the eye for spatial anisotropy. Here A is the azimuthal-averaged amplitude, and has a value of 19.8 nS for **d**, 2.81 M Ω for **e**, and 198 fA 2 /Hz for **f**. Setup conditions: **a**, $V_{set} = -5$ mV, $I_{set} = 200$ pA; **b** and **c**, $V_{set} = -1.3$ mV, $I_{set} = 520$ pA, $R_J = 2.5$ M Ω .

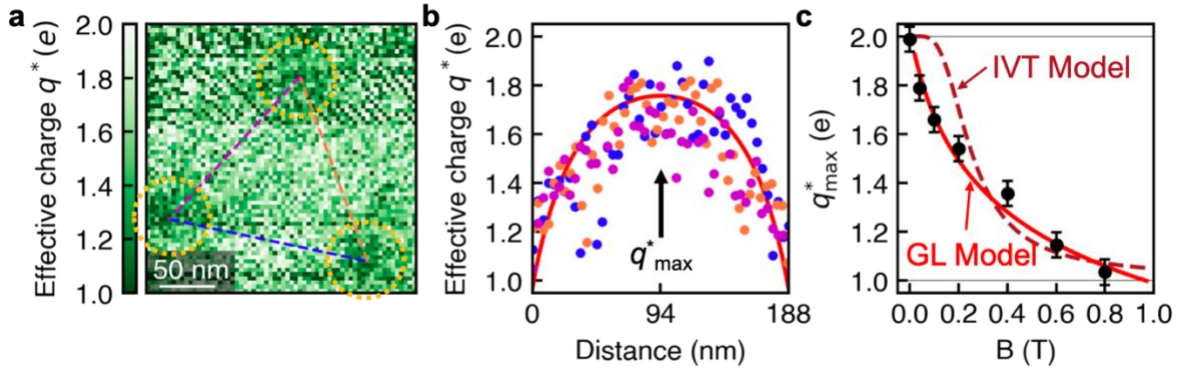


Fig. 4 Image of delocalized quasiparticles around three vortices. **a** Effective charge image measured at $eV_{\text{bias}} = \Delta_t$ and $B = 0.04$ T. The yellow dotted circles indicate the locations of three vortices (see Fig. S1). Setup conditions: $V_{\text{set}} = 1.3$ mV, $I_{\text{set}} = 520$ pA. **b** line profiles of effective charge along three linecuts between centers of vortex cores in **a**. **c** Magnetic field dependence of the maximal effective charge q^*_{\max} . The error bars are determined by the standard deviation of the extracted q^* in the energy ranges $(\Delta_t \pm 0.1$ meV) and $-(\Delta_t \pm 0.1$ meV) in Fig. S2. The red lines in **b** and **c** are the expected effective charge from GL model fit (Eq. 5), with $\xi = 12$ nm. Here the inter-vortex distance $d = 188$ nm. The brown dashed curve is the inter-vortex tunneling model following Eq. 4 in Ref. [9], with $B_{c2} = 4.0$ T.

Supplementary Materials for
Visualizing delocalized quasiparticles in the vortex state of NbSe₂

Jian-Feng Ge,¹ Koen M. Bastiaans,² Jiasen Niu,¹ Tjerk Benschop,¹ Maialen Ortego Larrazabal,³ Milan P. Allan^{1*}

¹ Leiden Institute of Physics, Leiden University, 2333 CA Leiden, The Netherlands

² Department of Quantum Nanoscience, Kavli Institute of Nanoscience, Delft University of Technology, 2628 CJ Delft, The Netherlands

³ Debye Institute for Nanomaterials Science, Utrecht University, 3508 TA Utrecht, The Netherlands

*Corresponding author. Email: allan@physics.leidenuniv.nl

Table of Contents

I. Explanation of effective charge for $|eV_{\text{bias}}| < \Delta_s$
Fig. S1 to Fig. S3

I. Explanation of effective charge for $|eV_{\text{bias}}| < \Delta_s$

Because the energy gap of our Pb tip is greater than that of NbSe₂, $\Delta_s < \Delta_t$, when the bias energy $|eV_{\text{bias}}| < \Delta_s$, multiple Andreev reflection takes place for an asymmetric superconductor-insulator-superconductor (SIS) junction^[39]. In the zero-field case, we do observe a further increase of effective charge from $2e$ for $|eV_{\text{bias}}| < \Delta_s \sim 1.1$ meV in Fig. 2f, which is a hint of multiple Andreev reflection.

On the contrary, we notice a clear difference for the finite-field case, the effective charge q^* first saturates between $1e$ and $2e$; only when $|eV_{\text{bias}}|$ is much lower than Δ_s the effective charge q^* starts to rise again, reaching above $2e$. The bias range $|eV_{\text{bias}}| < \Delta_s$ where $q^* < 2e$ hints the existence of $1e$ process in the tunneling current.

In the zero-temperature limit, one should not expect $1e$ process for $|E| < \Delta_s$, and the effective charge $q^* > 2e$. We believe this $1e$ process occurs because of thermal activation. The $1e$ process requires that both tip and sample have a finite density of quasiparticles at corresponding energy. On the tip side it is a microcrystal of Pb, and its quasiparticle density of states does not vanish because of our temperature. On the sample side between vortices, the quasiparticles are excited from magnetic field by comparing zero-field data, which can allow further thermal broadening. Therefore, the effective charge between $1e$ and $2e$ even for $|eV_{\text{bias}}| < \Delta_s$ is expected at a finite temperature, but the thermal broadening effect should be suppressed at lower temperatures.

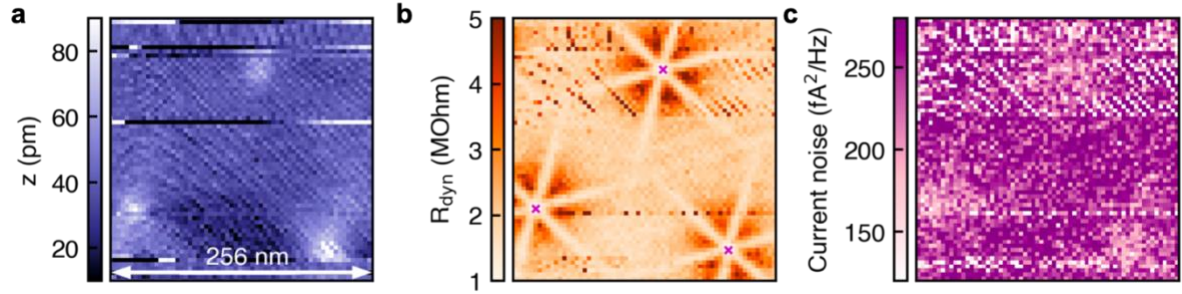


Fig. S1. Topography, dynamic resistance, and current noise image around three vortices. (a) Topographic image taken simultaneously around three vortices in the same field of view of Fig. 4a. (b) Dynamic resistance and (c) current noise imaged in the same field of view. (c) is further used to obtain Fig. 4a, the effective charge q^* image, by numerically solving Eq. 3. The crosses marked in (b) are used to determine the centers of vortex cores (dashed circles) in Fig. 4a. Setup conditions: $V_{\text{set}} = 1.3$ mV, $I_{\text{set}} = 520$ pA.

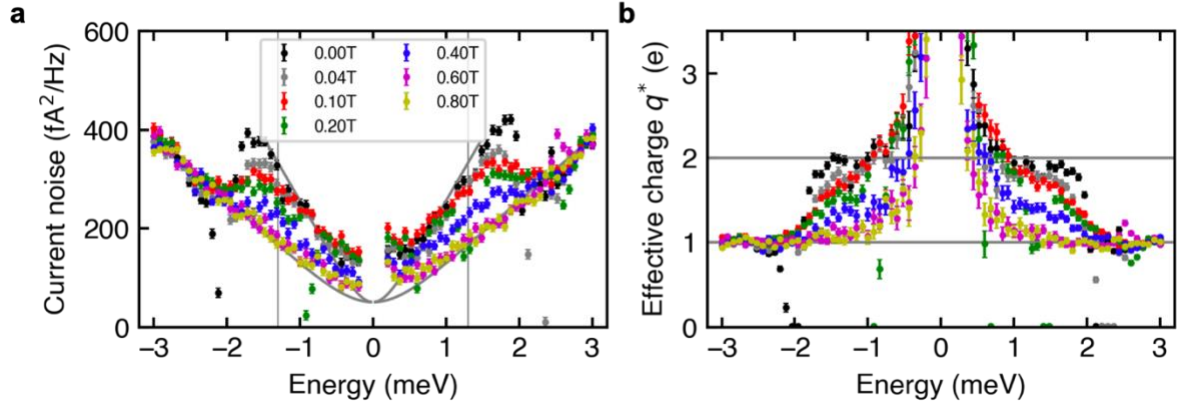


Fig. S2. Magnetic field dependence of noise spectra at the midpoint between vortices. (a) noise spectra and (b) the extracted effective charge at the midpoint between vortices (see Fig. S3) at various magnetic fields. The error bars are determined by the fluctuation of the current noise in time, yielding a standard deviation of $9.25 fA^2/Hz$. The gray lines in (a) indicate the gap energy of the tip $\pm \Delta_t$. The data points and error bars in Fig. 4c are determined by the mean and the standard deviation in the energy ranges $(\Delta_t \pm 0.1 \text{ meV})$ and $-(\Delta_t \pm 0.1 \text{ meV})$. Setup conditions: $R_J = 2.5 \text{ MOhm}$.

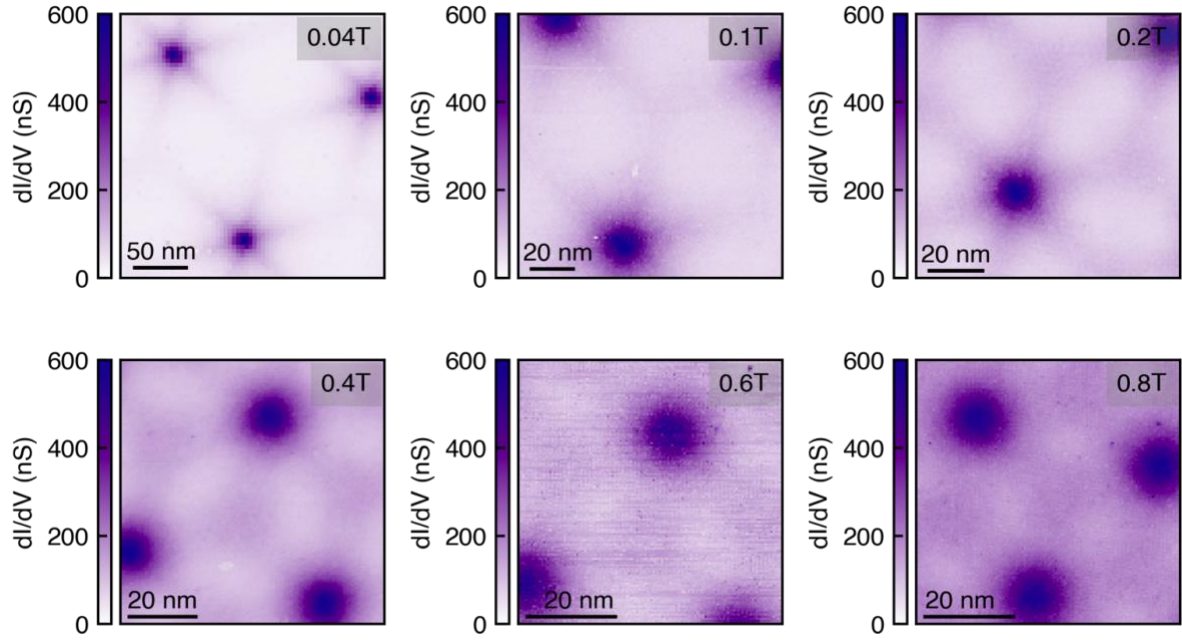


Fig. S3. Differential conductance image of vortices at different fields. Differential conductance images measured at $eV_{\text{bias}} = \Delta_t$ for the magnetic fields in Fig. 4 and Fig. S2. With these images we locate the midpoint between vortices at each field to take noise spectra. Setup conditions: $V_{\text{set}} = 1.3$ mV, $I_{\text{set}} = 520$ pA.